Arc Modeling Challenges

Rümpler Ch.[1], Narayanan V.R.T.[2]

[1]*Eaton, 1000 Cherrington Pkwy, Moon Township, PA 15108, USA*
[2]*Eaton, Bořivojova 2380, 252 63 Roztoky, Czech Republic*
ChristianRuempler@Eaton.com

Modeling of arcing phenomena has evolved towards becoming a state-of-the-art tool, supporting the design process of power distribution equipment in low-, medium-, and high-voltage applications. Modeling provides a better understanding of the physical processes within the devices which is needed in order to enhance product performance and mitigate risks in the development cycle. In this contribution, modeling challenges related to some of these applications are discussed: a) the calculation of thermodynamic and transport properties, b) the modeling approach for contact arm motion during arc interruption in low-voltage molded case circuit breakers (MCCB's), c) the model approach for arc flash events in medium-voltage (MV) switchgear.

Keywords: arc simulation, plasma transport properties, circuit breaker, switchgear

1 INTRODUCTION

Arcing phenomena are crucial in various applications in the power distribution system. Arcs are used either as a switching element, e.g. in circuit breakers with electromechanical contact systems or arcs occur as a fault event, e.g. as arc flash in low-voltage or medium-voltage switchgear. Due to the complex nonlinear processes associated with arcing phenomena, modeling has several useful aspects. A major factor for increased modeling activities in this field is the drive for miniaturization and cost reduction, which leads to increased power density and performance requirements. Here the model driven approach can help to optimize the design towards increased performance. Another aspect is the expensive testing done during development and certification. Having better confidence about the design helps to reduce expensive design-test cycles.

In this paper we discuss some of the challenging aspects related to the modeling of arc interruption and arc flash phenomena. Basis for any modeling approach are the necessary input data. In our MHD (magneto-hydrodynamics, [1]) based approach which is introduced in section 2, the thermodynamic and transport properties of the plasma are crucial input data. The calculation method and some results are discussed in the 3rd section. Furthermore, two application specific problems will be discussed, the contact arm motion modeling approach for low-voltage molded case circuit breakers (MCCB's) in section 4 and the modeling approach for arc flash in medium-voltage switchgear in section 5.

2 SIMULATION APPROACH

A modeling approach has been developed that covers the highly nonlinear physical processes during high-current arcing [2].

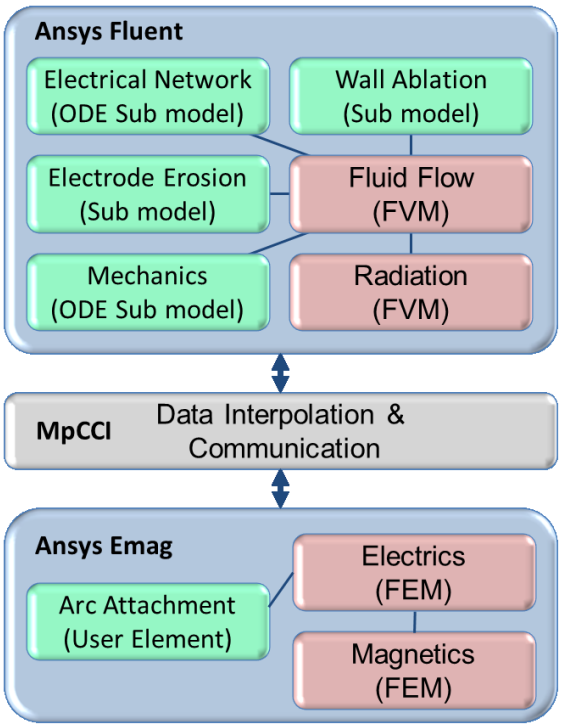

Fig. 1: Simulation system

The set of partial differential equations (PDEs) that describes the fluid flow, electromagnetic field, and radiation transport, respectively, are solved in a code coupling approach which is based on customized commercial solvers.

Splitting the calculation problem into separate tasks for fluid flow and electromagnetics enables a high performance solution. The basic setup of our simulation system is shown in fig. 1.

The mass, momentum, and energy balance equations as well as radiation equations are solved using a finite volume approach (FVM) by means of the ANSYS/Fluent solver [3]. Several sub models have been implemented as enhancements of the fluid flow (CFD) code, using the user programming interface the solver offers:

- An ordinary differential equation (ODE) can be solved in order to describe the interaction with the electric network that is connected to the modeled device.
- A model for the erosion of electrode material is used to calculate the mass of metal vapor that is ejected into the fluid region.
- Another sub model predicts the ablation of plastic materials [4].
- In case of MCCB modeling an ODE can be solved that predicts the rotational or translational motion of the contact arm, driven by magnetic forces.

To describe the electro-magnetic processes, the finite element approach (FEM) is used. Therefore the ANSYS/Emag [3] solver is customized, dividing the solution process into two steps, the solution of the electric and the magnetic equations. For the description of the arc attachment, a user defined element has been implemented that is able to represent the plasma sheath voltage drop [2].

The necessary data exchange and interpolation between the two mesh based codes is provided by the coupling server MpCCI [5].

3 PLASMA TRANSPORT PROPERTIES

In order to numerically model the arc dynamics within complex circuit breaker and switchgear geometries, accurate thermodynamic, transport and radiation properties of relevant gas mixtures are required as input. In this work, we primarily focus on calculating the thermodynamic and transport properties of air-metal vapor mixtures. The results will be provided for air-copper and air-tungsten mixtures, since copper-tungsten (Cu-W) is a commonly used alloy for metallic electrodes. The LTE-based transport properties are calculated following the works of Devoto [6, 7], in which the Chapman-Enskog formulation [8] for pure gases was extended to consider partially ionized and fully ionized gases. In this formulation, all the transport properties of interest can be obtained as a ratio of determinants of two matrices and the size of the matrices depends on the desired degree of accuracy (ζ) of the properties.

Calculation of collision integrals $\Omega_{ij}^{(l,s)}$ is an integral part of the Chapman-Enskog method, which requires the solution of equations (1)-(3).

$$\Omega_{ij}^{(l,s)} = \left(\frac{kT_{ij}^*}{2\pi\mu_{ij}}\right) \int_0^\infty e^{-\gamma_{ij}^2} \gamma_{ij}^{2s+3} \, Q_{ij}^{(l)} \, d\gamma_{ij} \qquad (1)$$

Here the superscripts (*l,s*) are related to coefficients of the Sonine polynomials. The integral collision cross section of l^{th} degree, associated with the collisional dynamics between "*i-j*" pair of species and dependent on the relative speed of collision g, is expressed as

$$Q_{ij}^{(l)}(g) = 2\pi \int_0^\infty \sigma(g,\chi)(1-cos^l\chi)\, sin\chi d\chi$$
$$= 2\pi \int_0^\infty (1-cos^l\chi)\, bdb\,, \qquad (2)$$

where $\sigma(g,\chi)$ is the differential collision cross section, b is the impact parameter, and χ is the angle of deflection given as

$$\chi = \pi - 2b \int_{r_{min}}^\infty \frac{dr}{r^2 \sqrt{\left(1-\frac{b^2}{r^2}-2\frac{\Phi_{ij}}{\mu_{ij}g^2}\right)}}\,. \qquad (3)$$

The most important parameter in equation (3) representing the collision dynamics is the interaction potential Φ_{ij} of the collision, which depends on the interaction partners *i* and *j*. In this work, while the elastic neutral-neutral and ion-neutral interactions have been characterized by the phenomenological Lennard-Jones potential [9], the shielded-Coulomb potential has been utilized for charge-charge collisions. Additionally, the contribution from inelastic charge-exchange interactions has been included for ion-parent neutral collisions using the approach suggested by Devoto. Finally, electron-impact momentum transfer cross sections

data are obtained from relevant databases for the electron-neutral interactions. The reduced mass μ_{ij}, reduced temperature T_{ij}^* and dimensionless kinetic energy γ_{ij} mentioned in equations (1)-(3) are given by

$$\mu_{ij} = \frac{m_i m_j}{m_i + m_j}$$
$$T_{ij}^* = \left[\frac{1}{m_i + m_j}\left(\frac{m_i}{T_j} + \frac{m_j}{T_i}\right)\right]^{-1}$$
$$\gamma_{ij} = \left(\frac{\mu_{ij} g^2}{2kT_{ij}^*}\right)^{\frac{1}{2}}. \quad (4)$$

In this section, we provide the transport properties results for air-copper and air-tungsten mixtures at atmospheric pressure, for different proportions of copper and tungsten vapors. The results for air-copper mixtures have already been validated in a previous work [10], while published data does not exist for air-tungsten mixtures to the best of the authors' knowledge.

Fig. 2 depicts the variation of the electrical conductivity σ with temperature for different mole fractions of copper and tungsten in air at 1 bar pressure. The following observations can be made:

i. The addition of Cu or W results in a significant increase in σ at temperatures lower than 15 kK compared to pure air (the red 0% Cu curve).
ii. Above 15000 K increasing content of copper and tungsten decrease σ compared to air.
iii. Tungsten content intensifies the behavior in both temperature ranges resulting in lower conductivity than copper for high temperatures and higher σ for temperatures below approximately 15000 K.

The observation (i) is of concern, since the increase in σ at lower temperatures due to metal vapor increases the joule heating effect and thereby can contribute to a thermal breakdown close to current zero in a circuit breaker.

The variation of dynamic viscosity with temperature for different copper and tungsten content is shown in fig. 3. The viscosity peaks for metal vapor mixtures are lower than that for pure air, while those for 50% and 100% Cu are lower than those for 50% and 100% W respectively.

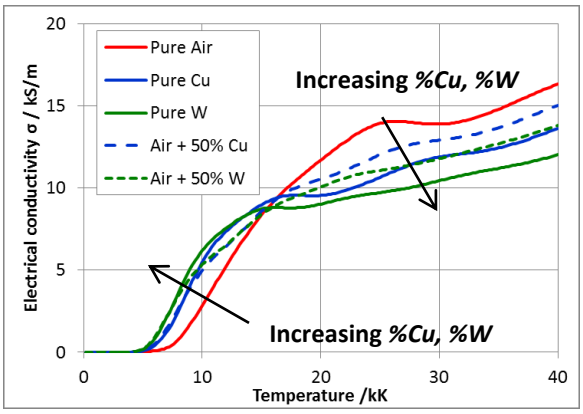

Fig. 2: Plot of electrical conductivity vs. temperature for different mole fractions of either Cu or W in air atmosphere

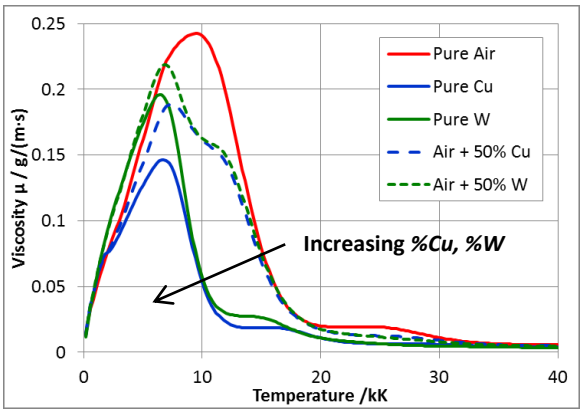

Fig. 3: Plot of viscosity vs. temperature for different mole fractions of Cu and W in air

The viscosity peaks are associated with the onset of ionization and subsequent creation of electrons and ions, thereby increasing the charge-charge cross section and reducing the mean free path. The importance of dynamic viscosity in arc simulations appears through Reynolds number (Re), which is the ratio of inertial and viscous forces. For a given geometry, a critical Reynolds number (Re_{crit}) can be determined based on simplifying assumptions. If the Reynolds number exceeds the critical limit ($Re > Re_{crit}$), a transition from laminar to turbulent flow occurs. Turbulent flows are well-known to drastically increase heat and mass transfer, and hence can efficiently cool and extinguish the arc.

Finally, the variation of total thermal conductivity with temperature for different copper and tungsten fractions is presented in fig. 4.

The total thermal conductivity is the sum of four different contributions: (i) heavy-species, (ii) electron, (iii) reactive, and (iv) internal thermal conductivities. The contribution from internal thermal conductivity is usually negligible in the entire temperature range, while at temperatures above 20 kK, the contribution from electron thermal conductivity dominates. The three peaks observed for air at 3.5 kK, 7.0 kK and 15 kK correspond to those for diatomic oxygen (O_2) dissociation, diatomic nitrogen (N_2) dissociation and combined first ionizations of atomic nitrogen (N) and oxygen (O), respectively. Increasing the fraction of metal vapor results in the decrease of all peak magnitudes; with all the peaks vanishing for pure Cu and W. The thermal conductivity of 50% Cu has been observed to be higher than that of 50% W at temperatures above 15 kK, while the thermal conductivity of pure Cu is observed to be higher than that of pure W at temperatures above 20 kK. Physically, thermal conductivity is important since it improves the conduction cooling within a circuit breaker and greater thermal conductivity results in a better gas cooling.

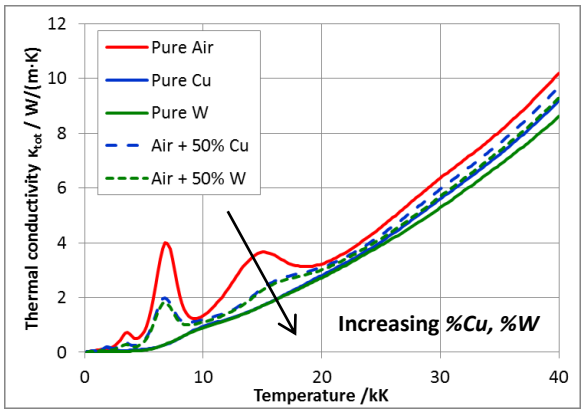

Fig. 4: Plot of thermal conductivity vs. temperature for different mole fractions of Cu and W in air

4 MCCB MOVING CONTACT ARM

For low-voltage molded case circuit breakers (MCCB's), the interruption of high short-circuit currents cause large thermal and mechanical stresses. Due to device miniaturization and increasing demands for higher performance, a prediction of the interruption process is needed to enable design optimization.

One challenge connected to the modeling of MCCB's is the representation of the contact arm motion. In fig. 5 a sketch of a double break contact system of a 630 A rated MCCB is shown, with two different contact arm positions, current path, indication of the arc positions, and two stacks of ferromagnetic splitter plates. In comparison to other contact designs, like in IEC type miniature circuit breakers, the arc burns relatively stable between the fixed and movable contact during contact opening. After a certain contact gap is achieved the arc is pushed by magnetic forces into the stack of splitter plates in order to quench and cool the arc.

For high short-circuit currents the design of these breakers depends on limiting the current to levels well below the prospective short-circuit current in order to reduce the stress on the installation. This is achieved by quickly raising the voltage of the arc above the line voltage through intensive arc cooling and lengthening of the arc by a combination of magnetic forces and fast opening of the movable contact arm. Breakers using this principle are referred to as current-limiting breakers. Because of this current limiting design principle, the contact motion and therefore arc elongation has a large impact on the arc voltage and interruption performance, since a fast arc voltage increase is needed for the limitation of the fault current.

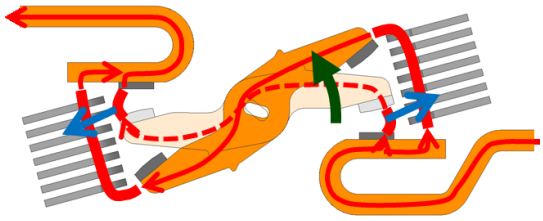

Fig. 5: Arm motion and arc lengthening in a MCCB double-break contact system (sketch)

Therefore the contact arm motion needs to be included in the model; otherwise the whole current limiting process cannot be predicted.

For the representation of moving objects in the FEM or CFD model, several different basic opportunities exist, as described in [11]:

- **Mesh deformation:** move contact arm nodes, use mesh morphing algorithm to deform other cells
- **Remeshing:** on the fly agglomeration or splitting of cells based on mesh quality metrics or remeshing of whole domain
- **Layering:** insertion or removal of cell layers
- **Overset grids:** Assembly of several overlapping movable structured grid blocks, interpolation of variables on the boundaries of the blocks
- **Mesh replacement:** Exchange parts or complete mesh with previously prepared mesh, interpolate data from old to new mesh

The selection of the most appropriate method for this application is based on several requirements. First of all the method needs to be easy to use since a complex setup of parameters or procedures is fault prone. Next an emphasis needs to be put on the performance, costly mesh related operations at every time step would limit the overall performance. Furthermore a high mesh quality needs to be assured at any time, since bad mesh quality as result of mesh changes introduces errors and could cause the solution to fail. Finally the method needs to be supported by the applied simulation tools, the CFD solver, FEM solver as well as the coupling tool.

All of these requirements could be met with the mesh replacement approach. Here we create all needed meshes upfront, where each mesh represents a certain contact position. While the simulation is running, meshes are swapped on the fly when needed to represent the motion of the contact. This involves the interpolation of the field values only when meshes are swapped.

Fig. 6 shows the mesh for different contact arm positions and compares morphing with mesh replacement approach. Starting from the mesh that represents the initial contact gap (fig. 6a) several morphing steps while opening the contact arm would lead to a deformed mesh with bad quality metrics. On the other hand, the mesh replacement (fig. 6b) offers high mesh quality any time, depending on the effort spent during mesh generation.

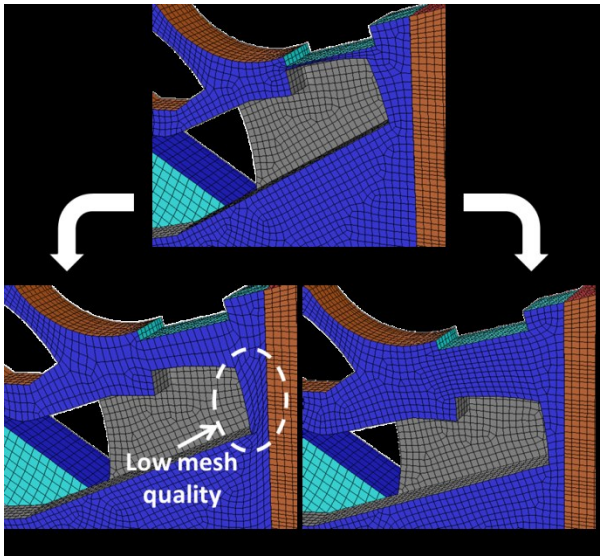

Fig. 6: Mesh at different contact arm position: a) initial contact gap, b) mesh after some morphing steps, c) mesh after several replacement steps

A challenging aspect is the fact that 3 codes have to support this procedure, and the mesh swap needs to be synchronized. When the CFD mesh is changed, the FEM mesh needs to be updated as well; also the neighborhood search that the coupling tool is evaluating to enable the data interpolation needs to be updated. Otherwise invalid data would be transferred between the codes, leading to an invalid solution (or a solver crash). A signal based communication scheme was implemented to handle this appropriately.

Model results highlighting the difference between a stationary mesh model and the mesh replacement approach are shown in fig. 7. For better comparison of measured and calculated voltage, the model result was low-pass filtered since the analog-digital converter used in the test has this characteristic. Therefore one disadvantage of our approach is not visible right away. Due to the small discrete steps that are used to define the contact arm position, the arc voltage also shows a stepwise profile rather than a continuous profile that would be expected by continuous arm motion, as shown in fig. 8. In order to smooth the voltage profile, the arm motion step size could be reduced or additional mesh morphing steps could be introduced.

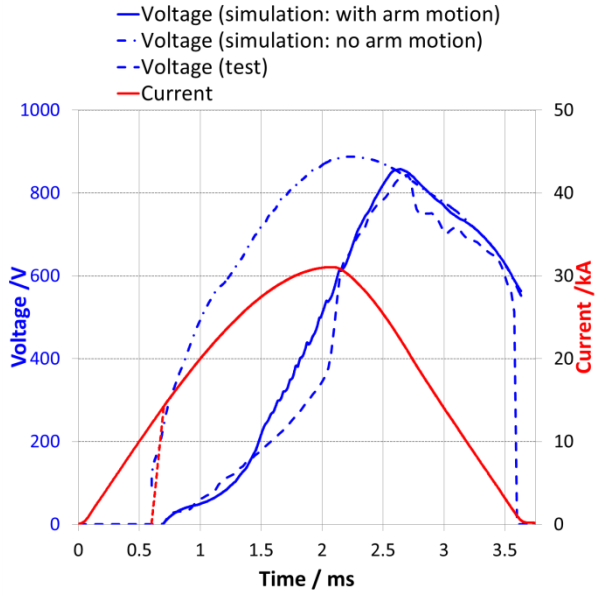

Fig. 7: Comparison of calculated and measured arc voltage, simulation with and without consideration of contact arm motion (440 V, 50 kA, 630 A breaker)

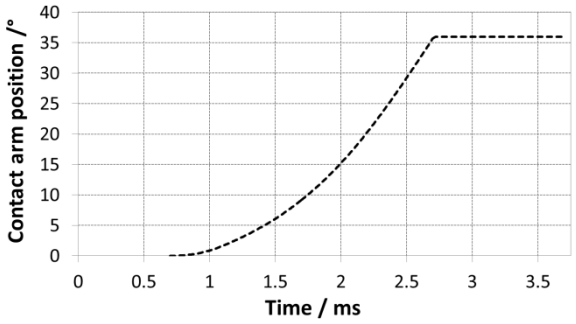

Fig. 8: Contact arm position vs. time curve

In case of no arm motion, the model represents the situation of completely opened contact over the entire duration of simulation. In this case the initial arc is defined as a long conductive channel with a small diameter between fixed and moveable contacts. In this model the current was used as a predefined load rather than as a result of the electric network ODE solver, to allow direct comparison between the two contact arm modelling approaches.

The ignition procedure in case of open contacts is not straightforward, since the long initial arcs lead to a high power input right at the beginning of the simulation, which is started at the time point where Lorentz forces exceed the contact spring forces (pop up current, here about 14 kA at 0.7 ms). In order to get the model running at all, it is necessary to ramp up the current from zero to the pop up current level in a short time (0.1 ms, see dashed current curve in fig. 7) rather than starting directly at 14 kA. The impact of the open contact position is clearly visible, comparing the voltage trace (simulation: no arm motion) with the measured voltage. Right at the beginning until about 2.5 ms the arc voltage is largely overestimated; therefore the arc energy (46 kJ vs. 24.9 kJ) as well, as shown in fig. 9. The current limiting would be overestimated as well, if this approach would be combined with the electric network ODE model.

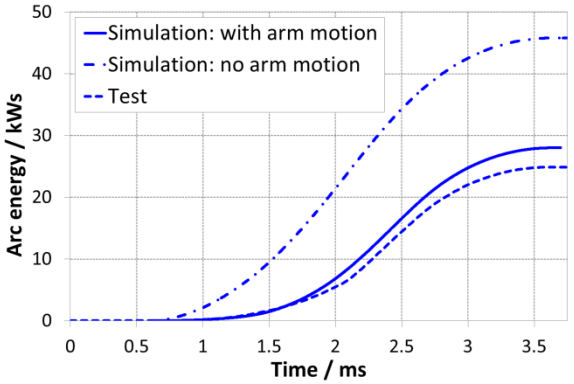

Fig. 9: Arc energy: simulation and test results

The result for the model that includes the contact arm motion is also shown in fig. 7. A much better representation of the arc voltage rise due to arc lengthening and delayed arc splitting in the splitter plates can be seen, in good agreement with the measurement results. With this arc voltage result, the arc energy prediction (28 kJ vs. 24.9 kJ) is much closer to the test results (fig. 9).

A visualization of the model result is given in fig. 10. The arc shape represented by a 12000 K iso-surface is shown for three different time points. In the initial time period (here 0.95 ms) the arc exists in the still small contact gap, which leads to an ejection of a hot plasma jet towards the splitter plates. This hot gas stream heats up the splitter plates, enhancing arc attachment and splitting later on when the arc is moving towards the plates. With increasing contact gap, the arc moves out of the contact gap towards the plates and is finally split into several arcs in the stack of plates, leading to a rapid increase of the arc voltage.

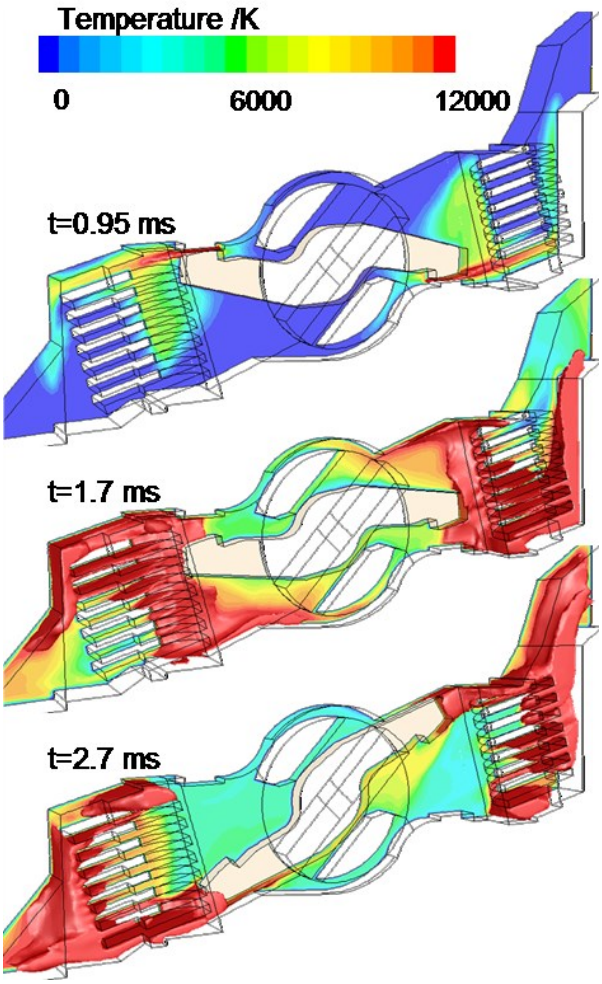

Fig. 10: Model result: temperature inside the MCCB chamber visualized by means of a 12000 K iso–surface (440 V, 50 kA, 630 A breaker)

5 MV SWITCHGEAR ARC FLASH

As a third example illustrating modeling challenges, an arc modeling approach for the prediction of arc flash events in medium-voltage (MV) arc flash resistant switchgear is discussed. A typical design of a MV switchgear section is shown in fig. 11.

IEC type arc resistant switchgear is tested according to IEC 62271-200 Annex A, where the switchgear has to withstand up to 1s of internal arcing, causing high mechanical and thermal stresses.

Because these tests are very expensive, various modeling approches have been developed in the past [12] in order to predict the mechanical loads (pressure rise) due to the arc flash to reduce the number of tests. With a simplified model that is based on the assumption of uniform distribution of temperature and pressure, prediction of the peak pressure is possible [13]. But in order to perform this calculation, values for the arc energy are needed as input, which are not available without initial testing so far.

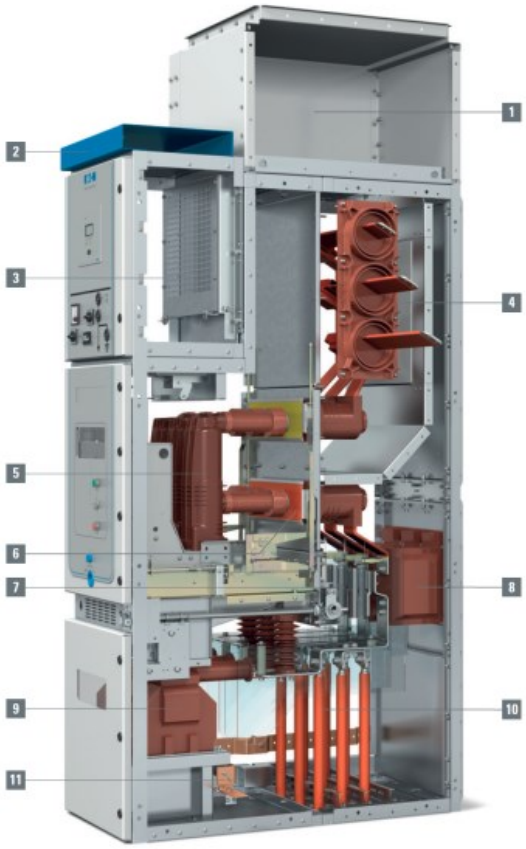

Fig. 11: Eaton MV switchgear: bus bar compartment (4), circuit breaker compartment (5), and cable compartment (10)

In case of a new design, the application of the 3D arc model is attractive, since arc energy as well as pressure rise can be predicted directly. Additionally, when solving beyond the initial arcing period of about 60 ms, thermal loads that could lead to a burn through e.g. of the side panels could also be predicted. But in comparison to a LV circuit breaker, the volume that has to be modeled is significantly larger (e.g. 100x) and the arcing time is much longer (e.g. 1000 ms vs. 10 ms). This leads to high computational cost with calculation time being a major challenge.

Fig. 12: Simplified test setup for arc flash experiments

To investigate the applicability, a simplified switchgear model as described in [14] has been used. The setup as shown in fig. 12 contains a compartment with two sections (1200 mm × 600 mm × 500 mm) with a venting chimney at the top (152 mm × 152 mm). Three electrodes are mounted in the lower section side by side with a gap of 85 mm between each other. In front of the electrodes a metal sheet is mounted where the arc can attach. The model results given in the following text are compared with test results obtained with an 18 kA asymmetrical short circuit current at 24 kV, as can be seen from fig. 13.

A 3D model has been created and calculation was performed for 60 ms of arcing time. In the experiment the arc was ignited with a copper wire across the three electrodes. In the model a conductive channel with 5 mm radius was defined as initial condition.

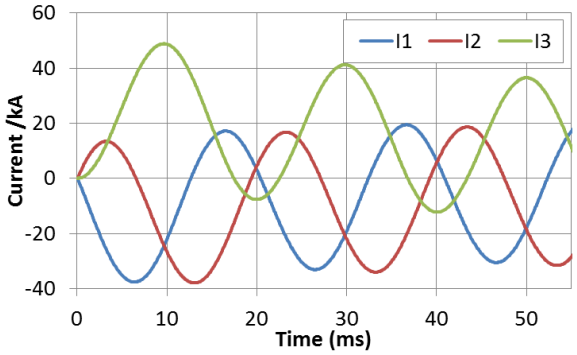

Fig. 13: Three-phase short circuit current

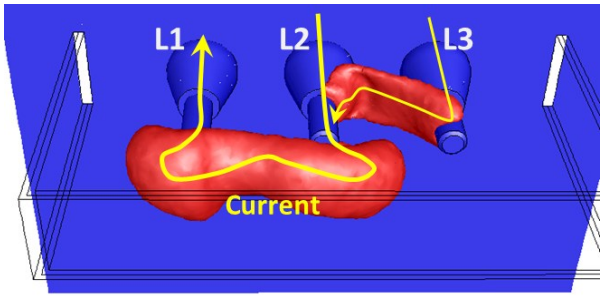

Fig. 14: Arc shape at t=2 ms (1000 K iso surface)

After ignition the arc is moved due to Lorentz forces, as seen in fig. 14. At 2 ms the arc between L1 and L2 bends away from electrodes and the arc between L2 and L3 bends towards the electrodes due to the current loops formed. Further on the arc elongates and attaches to the metal sheet in front of the electrodes, which causes the arc voltage to fluctuate due to the shortening of the arc length. The comparison of the phase-to-phase voltage from simulation and experiment is shown in fig. 15. Considering the complexity of the model, the achievable voltage prediction is sufficient, although the frequency of fluctuations in the simulation result exceeds the measurement results. But more important is the prediction capability with respect to the power and especially of the arc energy, since these values can be used for further investigation using reduced models (CFD or simplified model [12]). These values are given as model and test results in fig. 16. The overall level of arc power is sufficiently predicted and therefore the arc energy as well.

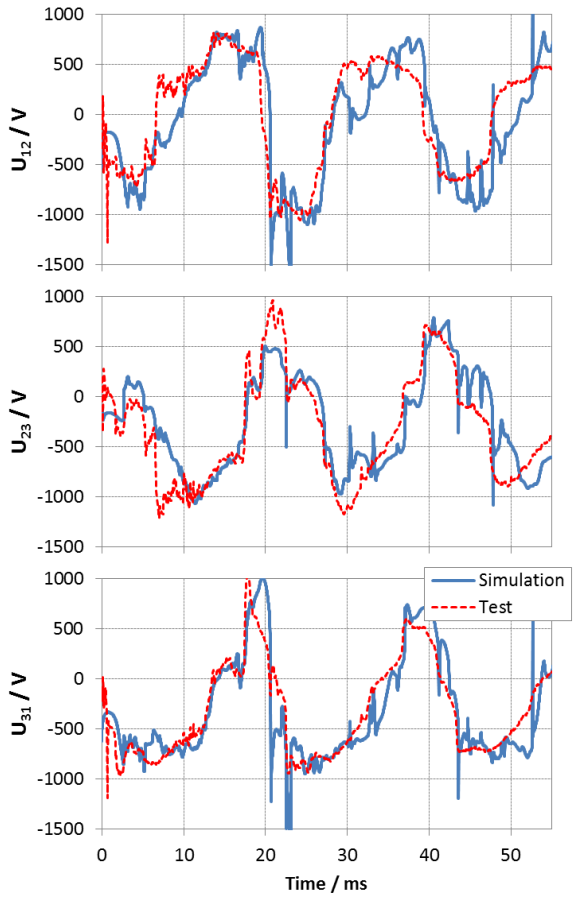

Fig. 15: Phase-to-phase arc voltage, simulation and test results

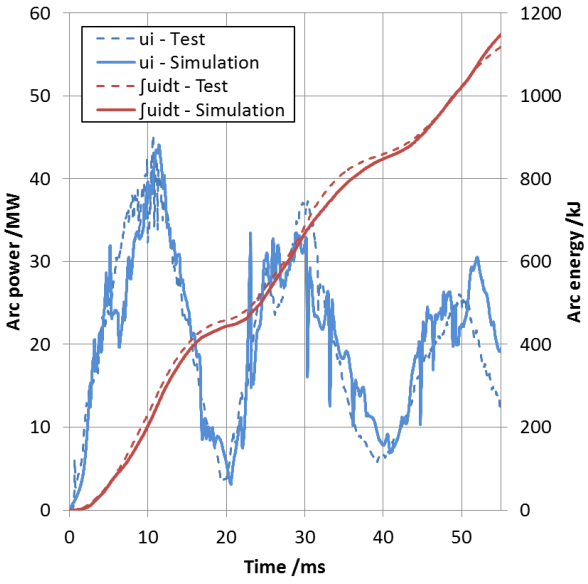

Fig. 16: Arc power and arc energy, comparison of simulation and test results

6 CONCLUSION

Numerical methods are used to predict the arc interruption in low-voltage circuit breakers and the fault arc in medium-voltage switchgear, where a number of challenges were addressed. Any simulation model needs input parameters which determine the result quality. In case of 3D MHD arc modeling the thermodynamic and transport properties of the plasma, composed of air and metal vapor in our case, are needed. A state of the art calculation approach has been discussed and results for copper and tungsten are presented.

The application of the model is presented for short-circuit interruption of low-voltage circuit breaker (MCCB) and medium voltage switchgear arc flash. In case of MCCBs, the contact motion needs to be modeled and the chosen mesh replacement method provides the best result quality with high-quality meshes prepared upfront. This avoids a solution dependency of the mesh related procedures which could lead to problems in a long running calculation. The arc flash modeling approach has been presented by means of a simplified compartment, showing the prediction opportunities for arc energy and arc power.

Acknowledgements

The authors wish to thank Mr. Albert Zacharias for performing calculations and Mr. Wilbert de Vries, Karl-Heinz Mayer and Brian E. Carlson for their continuous support of this effort.

REFERENCES

[1] Gleizes A, Freton P, Gonzalez J J, Journal of Physics D: Applied Physics 38 (2005) R153-R183.

[2] Rümpler Ch, Lichtbogensimulation für Niederspannungsschaltgeräte, Diisertation, Techn. Univ. Ilmenau, Frauenhofer Verlag, 2009.

[3] ANSYS, Inc., ANSYS, Release 15, Help system, Canonsburg, PA, USA, 2014.

[4] Rümpler Ch, Stammberg H, Zacharias A, Low-Voltage Arc simulation with Out-Gassing Polymers, In: 57th IEEE Holm Conference on Electrical Contacts, Minneapolis, MN, 2011.

[5] Frauenhofer Institute SCAI, MpCCI 4.4 Documentation, Sankt Augustin, 2015.

[6] Devoto R S, Physics of Fluids 9 (1966) 1230-1240.

[7] Devoto R S, Physics of Fluids 10 (1967) 2105-2211.

[8] Chapman S, Cowling T G, The Mathematical Theory of Non-uniform Gases, Cambridge University Press, 1970.

[9] Pirani F, Alberti M, Castro A, Moix Teixidor M, Cappelletti D, Chemical Physics Letters 394

(2004) 37-44.
[10] Narayanan V R T, Numerical modeling of post current-zero dielectric breakdown in a low voltage circuit breaker, PhD dissertation, University of Minnesota, 2014.
[11] Rümpler Ch, Zacharias A, Stammberger H, Low-voltage circuit breaker arc simulation including contact arm motion, In: 27th International Conference on Electrical Contacts, Dresden, Germany, 2014.
[12] CIGRE, Tools for the simulation of effects of the internal arc in transmission and distribution, CIGRE WG A3.24, January 26, 2014.
[13] Uzelac N, Dullni E, Kriegel M, Pater R, Application of simplified model for the calculation of the pressure rise in MV switchgear due to internal arc fault, In: 22nd International Conference on Electricity Distribution (CIRED 2013), Stockholm, 2013.
[14] IEEE Power & Energy Society Switchgear Committee, C37.20.7 Working Group Report, IEEE, October 11, 2011.